JCTC Journal of Chemical Theory and Computation

Feynman−Kleinert Linearized Path Integral (FK-LPI) Algorithms for Quantum Molecular Dynamics, with Application to Water and He(4)

Jens Aage Poulsen,*,† Gunnar Nyman,† and Peter J. Rossky‡

Physical Chemistry, Göteborg University, S-412-96, Göteborg, Sweden, and Institute for Theoretical Chemistry, Department of Chemistry and Biochemistry, University of Texas at Austin, Austin, Texas 78712

Received May 11, 2006

Abstract: The Feynman−Kleinert Linearized Path Integral (FK-LPI) representation of quantum correlation functions is extended in applications and algorithms. Diffusion including quantum effects for a flexible simple point charge model of liquid water is explored, including new tests of internal consistency. An ab initio quantum correction factor (QCF) is also obtained to correct the far-infrared spectrum of water. After correction, a spectrum based on a classical simulation is in good agreement with the experiment. The FK-LPI QCF is shown to be superior to the so-called harmonic QCF. New computational algorithms are introduced so that the quantum Boltzmann Wigner phase-space density, the central object in the implementation, can be obtained for arbitrary potentials. One scheme requires only that the standard classical force routine be replaced when turning from one molecular problem to another. The new algorithms are applied to the calculation of the Van Hove spectrum of liquid He(4) at 27 K. The spectrum moments are in very good agreement with the experiment. These observations indicate that the FK-LPI approach can be broadly effective for molecular problems involving the dynamics of light nuclei.

1. Introduction

Recently, a variety of computational schemes such as centroid molecular dynamics (CMD),[1,2] ring polymer molecular dynamics (RPMD),[3,4] forward−backward semiclassical dynamics,[5] the classical Wigner (CW) model,[6−10] mode coupling theory,[11] and analytic continuation methods[12] have been applied for modeling real many-body quantum dynamical processes in the condensed phase. Common to all of these methods is the focus on the time correlation function (CF) formalism: The process of interest is studied by evaluating its corresponding CF. For instance, the dynamic structure factor in neutron or X-ray scattering experiments is described by a Van Hove CF, and the rate of diffusion of a particle is obtained from its velocity CF. The accuracy of the different methods remains difficult to evaluate, but it appears that they are all able to capture the main qualitative quantum effects that are relevant in a condensed phase, where quantum coherences are quenched because of the strong interatomic couplings.

The CW model, the subject of this paper, is perhaps conceptually the simplest of the methods considered above and has a rigorous derivation.[9] It has been successfully applied for obtaining vibrational relaxation rates of oxygen in liquid oxygen, determined by the golden rule force−force CF,[10] the diffusion coefficient for liquid para-hydrogen at 17 and 25 K, via the Kubo velocity CF,[8] neutron scattering via the Van Hove CF of liquid He(4) at 27 K,[6] and the diffusion coefficient plus a quantum correction factor for the infrared spectrum of water.[7] In short, the model splits the calculation of the quantum CF into two separate tasks, the generation of initial conditions and the propagation of dynamics. The sampling of the appropriate quantum initial conditions (here assumed to be given by a Boltzmann operator) is done through Wigner's phase-space distribution,

* Corresponding author e-mail: jens72@chem.gu.se.
† Göteborg University.
‡ University of Texas at Austin.

10.1021/ct600167s CCC: $33.50
Published on Web 09/28/2006

while the dynamics are approximated as classical (the single, but great, simplification); see eq 1 below. To derive the CW method, one expresses the CF as a Feynman path integral (PI) and linearizes the action difference between the forward−backward time paths.[9,13] This *linearized path integral* (LPI) approximation, which is common to several recently proposed dynamics methods,[9,13−16] can be justified by a strong coherence loss for systems in which the dynamics of many degrees of freedom are relatively well-coupled to the degree of freedom being probed; see ref 9 for further details.

To make the computation of the Wigner-transformed Boltzmann operator tractable, one may recast the latter in a semianalytical form through the variational effective frequency theory as introduced by Giachetti and Tognetti[17] and independently by Feynman and Kleinert[18] (hereafter FK). A key ingredient in the FK theory is the concept of a Feynman path centroid and an effective potential, the centroid potential. Feynman's centroid also plays a central role in CMD.[1,2] The special LPI implementation with its FK-based Wigner transform is denoted FK-LPI.[9] In the following, the acronyms LPI and CW will be used interchangeably, as they are formally equivalent.

In this paper, we apply the FK-LPI method to a realistic model of liquid water based on a simple point charge (SPC) model. We have already reported some results of a similar water study,[7] but here, the focus is a bit different: not only is the new water sample twice as large as the old one, but we also now focus explicitly on the consistency of the various FK-LPI CFs and compare the performance of a FK-LPI-based quantum correction factor (QCF) with the so-called harmonic QCF, when both are applied to correct the far infrared spectrum of water obtained by classical molecular dynamics. The consistency tests among alternative routes to a CF are not, in general, accessible in other schemes.

In the FK-LPI implementation, it is the computation of the centroid potential which is the computationally most demanding part, as discussed below. In some special cases, for example, for potentials that can be expressed by Gaussian functions or in a Fourier series, one may still derive analytic formulas for the centroid potential, but for general potentials, this is not possible. In this paper, we present computational schemes for determining the FK centroid potential—and thereby the Wigner-transformed Boltzmann operator—for systems described by *arbitrary* potentials. The implementations are sufficiently general to permit a user to make only small changes to a FK-LPI code when migrating from one physical problem to another. Indeed, one is only required to substitute one potential gradient routine for another, when shifting from, for example, SPC water to a He(4) liquid. We report such "black box" implementations of the FK-LPI theory to the determination of the spectrum of density fluctuations in liquid He(4) at 27 K, the first realistic problem to which the FK-LPI theory was applied.[6]

This paper is structured as follows. In section 2, we describe the FK-LPI theory and its general implementation. Section 3 contains a description of the specific FK-LPI water and He(4) implementations. In section 4, we report and compare FK-LPI results for the water quantum liquid structure, nuclear velocity, and infrared spectrum to both the predictions of classical mechanics and experimental results. Also, we present the results of the "black box" implementations of FK-LPI when applied to the He(4) problem. We conclude in section 5 with a summary and further comment on the outlook for future applications of the method.

2. Theory and Implementation.

In this section, we present the basic equations of the FK-LPI method and review the iterative FK equations which must be solved in order to set up the Boltzmann Wigner transform. The "black box" versions of the FK equations are introduced, and finally, a brief introduction to the He(4) dynamic structure factor is given.

2.1. The Classical Wigner or LPI Approach. The LPI approach to the computation of quantum CFs is perhaps the simplest one to express. The precise expression that is derived from the linearization approximation seems to have appeared first in the work of Hernandez and Voth[14] and was developed independently as the linearized semiclassical initial value representation by Sun and Miller.[19] The LPI approximation to the CF $\langle \hat{A}(0)\hat{B}(t)\rangle$ is simply

$$\langle \hat{A}(0)\hat{B}(t)\rangle \approx \frac{1}{(2\pi\hbar)^{3N}} \int\int \frac{dq\, dp}{Z} (\exp(-\beta\hat{H})\hat{A})_W[q, p](\hat{B})_W[q_t, p_t] \quad (1)$$

which follows *directly* from the exact PI expression when carrying out the linearization procedure. Equation 1 may be interpreted/implemented as follows: Phase-space points (q, p) are sampled from the Wigner transform of $\exp(-\beta\hat{H})\hat{A}$, the transform being defined for an arbitrary operator $\hat{C}$ by

$$(\hat{C})_W[x, p] \equiv \int_{-\infty}^{+\infty} d\eta \exp(-ip\eta/\hbar)\left\langle x + \frac{1}{2}\eta\middle|\hat{C}\middle|x - \frac{1}{2}\eta\right\rangle \quad (2)$$

(q, p) are evolved classically according to the Hamiltonian $H(q, p)$ to (q_t, p_t), which serve as the phase-space arguments of $(\hat{B})_W[q_t, p_t]$. $3N$ is the dimensionality of the problem.

2.2. Feynman−Kleinert Wigner Transform. Recently, we suggested a practical route to the Wigner transform of the $\exp(-\beta\hat{H})\hat{A}$ operator, which is required by LPI.[9] This approach was based on combining the novel effective frequency variational theory of Feynman and Kleinert (FK)[18] with the quasi-density operator formalism of Jang and Voth.[1,20] The approach exploits the classical centroid phase-space variables (x_c, p_c), where

$$x_c = \frac{1}{\beta\hbar}\int_0^{\beta\hbar} d\tau x(\tau) \quad (3)$$

and p_c is the corresponding centroid momentum. Presented in formal terms, in one dimension, one may approximate the Boltzmann operator by[9]

$$\exp(-\beta\hat{H}) \simeq \int\int dx_c\, dp_c\, \rho_{FK}(x_c, p_c)\, \hat{\delta}_{FK}(x_c, p_c) \quad (4)$$

where $\rho_{FK}(x_c, p_c)$ is the FK approximation to the centroid phase-space density:

$$\rho_{FK}(x_c, p_c) = \frac{1}{2\pi\hbar}\exp\left(-\beta\frac{p_c^2}{2M}\right)\exp[-\beta W_1(x_c)] \quad (5)$$

and $W_1(x_c)$ is the corresponding FK approximation to the centroid potential. The operator $\hat{\delta}_{FK}(x_c, p_c)$ is the so-called effective frequency quasi-density operator (QDO):

$$\hat{\delta}_{FK}(x_c, p_c) = \int\int dx\, dx' \sqrt{\frac{M\Omega(x_c)}{\pi\hbar\alpha}} \left|x'\right\rangle\!\left\langle x\right| \exp\left\{\frac{p_c}{i\hbar}(x' - x) - \frac{M\Omega(x_c)}{\hbar\alpha}\left(\frac{x+x'}{2} - x_c\right)^2 - \frac{M\Omega(x_c)\alpha}{4\hbar}(x' - x)^2\right\} \quad (6)$$

where α is a function of the *effective* frequency, $\Omega(x_c)$, through the relation

$$\alpha = \coth\left[\frac{\Omega(x_c)\hbar\beta}{2}\right] - \frac{2}{\Omega(x_c)\hbar\beta} \quad (7)$$

and the quantity α is related to the *smearing width* $a^2(x_c)$[18] through

$$a^2(x_c) = \hbar\alpha/2M\Omega(x_c) \quad (8)$$

This width measures the thermal quantum "fuzziness" around the classical-like position x_c. To close the equations, the effective frequency is given by the mass-weighted classical Hessian averaged over the length $a^2(x_c)$:

$$\Omega^2(x_c) = \frac{1}{M}\int dy \frac{1}{\sqrt{2\pi a^2(x_c)}} V''(x_c + y) \exp\left[-\frac{1}{2}y^2/a^2(x_c)\right] \quad (9)$$

This FK prescription gives the best local harmonic description of the potential surface, on the basis of a system free energy criterion.[18] To obtain $\Omega^2(x_c)$ and $a^2(x_c)$, eqs 7−9 must be solved iteratively, as discussed in the next section. Wigner-transforming eq 4 then amounts to transforming $\hat{\delta}_{FK}$, eq 6, which can be done analytically:

$$[\hat{\delta}_{FK}(x_c, p_c)]_W[q, p] = \frac{2}{\alpha}\exp\left[-\frac{M\Omega(x_c)}{\hbar\alpha}(q - x_c)^2 - \frac{1}{M\Omega(x_c)\alpha\hbar}(p - p_c)^2\right] \quad (10)$$

Further, if $\hat{A}$ is a relatively simple phase-space operator, the transform of $\exp(-\beta\hat{H})\hat{A}$ can also be obtained. For details, we refer to ref 9.

2.3. Feynman-Kleinert Iterative Equations. It is in principle easy to generalize the effective frequency theory to many dimensions; see, for example, ref 24. In the multidimensional formulation, the effective frequency matrix $\underline{\Omega^2(\vec{z}_c)}$ and the smearing width matrix $\underline{\mathbf{A}(\vec{z}_c)}$ [the $3N \times 3N$ dimensional generalizations of $\Omega^2(x_c)$ and $a^2(x_c)$, respectively], defined for a position $\vec{z}_c$, are determined through two self-consistent equations:

$$\underline{\Omega^2(\vec{z}_c)} = \int d\vec{z} \frac{1}{\sqrt{||2\pi\underline{\mathbf{A}(\vec{z}_c)}||}} \underline{\mathbf{M}}^{-1/2}\underline{\boldsymbol{H}_V(\vec{z})}\underline{\mathbf{M}}^{-1/2} \exp\left[-\frac{1}{2}(\vec{\mathbf{z}} - \vec{z}_c)^T\mathbf{A}(\vec{z}_c)^{-1}(\vec{\mathbf{z}} - \vec{z}_c)\right] \quad (11)$$

and

$$\underline{U}^\dagger(\vec{z}_c)\underline{\mathbf{M}}^{1/2}\underline{\mathbf{A}(\vec{z}_c)}\underline{\mathbf{M}}^{1/2}\underline{\mathbf{U}(\vec{z}_c)} = \underline{\Lambda} \quad (12)$$

where

$$\underline{\Lambda}_{ij} = \delta_{ij}\left\{\frac{k_BT}{\Omega_i^2(\vec{z}_c)}\left[\frac{\hbar\Omega_i(\vec{z}_c)}{2k_BT}\coth\left(\frac{\hbar\Omega_i(\vec{z}_c)}{2k_BT}\right) - 1\right]\right\} \quad (13)$$

In these equations, $\underline{\boldsymbol{H}_V(\vec{z})}$ is the $3N \times 3N$ classical Hessian matrix of the potential, $\underline{\mathbf{M}^{1/2}}$ is the diagonal matrix of the square root of masses, and $\Omega_i(\vec{z}_c)$, $i = 1$ and $3N$, is the square root of eigenvalues of $\underline{\Omega^2(\vec{z}_c)}$. $\underline{\mathbf{U}(\vec{z}_c)}$ is the matrix which diagonalizes $\underline{\Omega^2(\vec{z}_c)}$ and hence defines the effective frequency normal modes through

$$\vec{\eta} = \underline{U}^\dagger(\vec{z}_c)\underline{\mathbf{M}}^{1/2}\,\vec{z} \quad (14)$$

where $\vec{z}$ holds the usual Cartesian coordinates.

In practice, eqs 11−12 are solved as follows: Let $\vec{z}_c$ be given. Assume that the correct effective frequency matrix $\underline{\Omega^2(\vec{z}_c')}$ has been found in a geometry $\vec{z}_c'$ close to $\vec{z}_c$, for example, from a previous step in a Metropolis Monte Carlo (MC) walk on the centroid potential. Then, the steps are (i) diagonalize the effective frequency matrix to obtain an approximate $\underline{\mathbf{U}(\vec{z}_c)}$ matrix and vector of frequencies $\Omega_i(\vec{z}_c)$. (ii) Use eq 13 followed by eq 12 to obtain $\underline{\mathbf{A}(\vec{z}_c)}$. (iii) Equation 11 gives a new effective frequency matrix $\underline{\Omega^2(\vec{z}_c)}$. One then returns to step i until self-consistency for $\underline{\Omega^2(\vec{z}_c)}$ and $\underline{\mathbf{A}(\vec{z}_c)}$ is reached. In practice, only a few iterations are necessary. Once the effective frequencies and normal modes are obtained, the centroid potential is calculated according to[18]

$$W_1(\vec{z}_c) = k_BT\sum_{i=1}^{3N}\ln\left\{\frac{\sinh\left[\frac{\hbar\Omega_i(\vec{z}_c)}{2k_BT}\right]}{\frac{\hbar\Omega_i(\vec{z}_c)}{2k_BT}}\right\} + V_{A(\vec{z}_c)} - \frac{1}{2}\sum_{i=1}^{3N}\Lambda_{ii}\Omega_i^2(\vec{z}_c) \quad (15)$$

with the smeared potential given by the Gaussian average

$$V_{A(\vec{z}_c)} = \int d\vec{z} \frac{1}{\sqrt{||2\pi\underline{\mathbf{A}(\vec{z}_c)}||}} V(\vec{\mathbf{z}}) \exp\left[-\frac{1}{2}(\vec{\mathbf{z}} - \vec{z}_c)^T\mathbf{A}(\vec{z}_c)^{-1}(\vec{\mathbf{z}} - \vec{z}_c)\right] \quad (16)$$

Also, one may set up the Boltzmann Wigner transform, compare eq 10:

$$[\hat{\delta}_{FK}(\vec{z}_c, \vec{p}_c)]_W[\vec{q}, \vec{p}] = \prod_{i=1}^{3N}\frac{2}{\alpha_i} \exp\left[-\frac{\Omega_i(\vec{z}_c)}{\alpha_i\hbar}(\eta_i - \eta_{i,c})^2 - \frac{1}{\Omega_i(\vec{z}_c)\alpha_i\hbar}(\nu_i - \nu_{i,c})^2\right] \quad (17)$$

with the mass-weighted position and momentum normal modes, η_i and ν_i, being the ith entries of

$$\vec{\eta} = \underline{U}^\dagger(\vec{z}_c)\underline{\mathbf{M}}^{1/2}\vec{q}, \qquad \vec{\nu} = \underline{U}^\dagger(\vec{z}_c)\underline{\mathbf{M}}^{-1/2}\vec{p} \quad (18)$$

respectively. Two corresponding relations define $\eta_{c,i}$ and $\nu_{c,i}$ from the Cartesian centroid coordinates and momenta:

$$\vec{\eta}_c = \underline{U}^{\dagger}(\vec{z}_c)\underline{\mathbf{M}}^{1/2}\vec{z}_c, \qquad \vec{\nu}_c = \underline{U}^{\dagger}(\vec{z}_c)\underline{\mathbf{M}}^{-1/2}\vec{p}_c \quad (19)$$

2.4. General Implementations of the FK Equations. The major difficulty encountered in applying the FK-LPI method is the evaluation of eq 11, the smeared Hessian, and to a smaller extent, eq 16, the smeared potential. In this paper, we consider liquids described by nonpolarizable potentials, where efficient analytical expressions for these equations can be derived, see below. However, the derivation of the analytic equations require a fair amount of algebra, and alternative ways of solving the iterative FK equations for general potentials are desirable. Below, we consider two new implementations of the iterative equations which—to various degrees—eliminate the algebraic problem and extend the types of potentials accessible.

2.4.1. Hessian Sampling. A general way to evaluate eqs 11 and 16 would be to sample the classical Hessian and potential numerically. Thus, first, the multidimensional Gaussian sampling function, which is identical in these equations, is rephrased in normal mode coordinates, eq 14, which makes the Gaussian factorize. Then, one samples normal mode displacements from this Gaussian via Box−Muller sampling,[25] and these are converted back to Cartesian coordinates for evaluation of the Hessian or potential. As we shall see in a moment, this procedure works extremely well if one has an analytic Hessian at hand, which is usually possible if the potential is nonpolarizable. The method then needs routines directly providing both the classical Hessian and potential.

2.4.2. Gradient Sampling. This procedure only requires a routine that provides the potential and its gradient. These are available in any molecular dynamics code. To derive this method, we start by integrating eq 11 by parts, which leads immediately to

$$\underline{\Omega}^2(\vec{\mathbf{z}}_c) = \int \mathrm{d}\vec{\mathbf{z}}\, \frac{1}{\sqrt{||2\pi\underline{\mathbf{A}}(\vec{\mathbf{z}}_c)||}}\underline{\mathbf{M}}^{-1/2}\underline{\Delta}(\vec{\mathbf{z}}, \vec{z}_c)\underline{\mathbf{M}}^{-1/2} \exp\left[-\frac{1}{2}(\vec{\mathbf{z}} - \vec{z}_c)^T\mathbf{A}(\vec{\mathbf{z}}_c)^{-1}(\vec{\mathbf{z}} - \vec{z}_c)\right] \quad (20)$$

where

$$\underline{\Delta}_{ij}(\vec{\mathbf{z}}, \vec{z}_c) = \{\sum_{k=1}^{3N}(\underline{A}^{-1})_{kj}(z_k - z_{c,k})\} \times \frac{\partial}{\partial z_i}V(\vec{\mathbf{z}}) \quad (21)$$

Hence, the scheme for calculating the smeared Hessian requires sampling vectors $\vec{\mathbf{z}}$ around $\vec{z}_c$ and averaging to obtain the $(3N)^2$ quantities

$$\Gamma_{ij} = \left\langle (z_i - z_{c,i})\frac{\partial}{\partial z_j}V(\vec{\mathbf{z}})\right\rangle \quad (22)$$

The (i,j)th element of the smeared Hessian is then given by

$$\underline{\Omega}_{i,j}{}^2(\vec{z}_c) = m_i^{-1/2}m_j^{-1/2}\sum_{k=1}^{3N}\{\underline{A}^{-1}\}_{kj}\Gamma_{ki} \quad (23)$$

In practice, because of statistical errors in any finite sampling sequence, $\underline{\Omega}_{i,j}{}^2(\vec{z}_c)$ will not be symmetric, and this can be enforced by a "symmetrization" procedure:

$$\underline{\Omega}_{i,j}{}^2(\vec{z}_c) \rightarrow [\underline{\Omega}_{i,j}{}^2(\vec{z}_c) + \underline{\Omega}_{j,i}{}^2(\vec{z}_c)]/2 \quad (24)$$

2.5. Dynamic Structure Factor. The spectrum of density fluctuations—or equivalently the dynamic structure factor—may be defined for the reciprocal lattice vector $\vec{\mathbf{Q}}$ through[26]

$$S(\vec{\mathbf{Q}},\omega) = \frac{1}{2\pi}\int_{-\infty}^{+\infty}\mathrm{d}t\, \exp(-i\omega t)S(\vec{\mathbf{Q}}, t) \quad (25)$$

where the Van Hove CF is given by[26]

$$S(\vec{\mathbf{Q}}, t) = \frac{1}{N}\sum_{j,k=1}^{N}\langle \exp[-i\vec{\mathbf{Q}}\vec{r}_j(0)]\, \exp[i\vec{\mathbf{Q}}\vec{r}_k(t)]\rangle \quad (26)$$

The dynamic structure factor is experimentally accessible through neutron or X-ray scattering experiments. From the experiment,[27] one may extract the first three moments (time derivatives) of $S(\vec{\mathbf{Q}},\omega)$ ($S(\vec{\mathbf{Q}}, t)$). These moments thus serve as a link between the experiment and simulation.

In any liquid model that employs periodic boundary conditions, the reciprocal lattice vector must fulfill the Laue equation: $Q \times L = 2\pi n$, where Q is a component of $\vec{\mathbf{Q}}$, L is the box length in that direction, and n is an integer.

3. Water and He(4) FK-LPI Molecular Dynamics Implementation.

3.1. Water Potential and Its Implementation in the Iterative FK Equations. The liquid water model is constructed by adopting the SPC model of Berendsen et al.[28] In the SPC model, the water interactions are described by Lennard-Jones (LJ) interactions between oxygen atoms (ϵ = 78.22 K; σ = 3.165 Å) and an electrostatic Coulomb potential between atoms on different molecules, the latter defined by charges $0.41e$ and $-0.82e$, on hydrogen and oxygen, respectively. A flexible water model is introduced by adopting the harmonic part of the local mode intramolecular water potential of Reimers and Watts,[29] see eq 30 below. The water monomer geometry is put equal to the equilibrium geometry of the original rigid SPC model. In the following, we will refer to the model as SPCf (f for flexible). We will make no effort to reparametrize the SPCf potential parameters in the current work, in order, for example, to develop a model which agrees better with the experiment after quantization.

To handle the long-range electrostatic interactions, the Ewald summation method is adopted with conducting tin foil boundary conditions. For an exceptionally clear and pedagogical account of the Ewald summation technique, see the user's guide and manual of the MOSCITO simulation package.[30] In the real space part, we employ the standard approximation of including only the central box in the summation. A total of 337 reciprocal space vectors corresponding to $\vec{\mathbf{k}} = 2\pi(n_x, n_y, n_z)/L$, $n_x^2 + n_y^2 + n_z^2 \leq 27$ are utilized in the Ewald reciprocal space sum, and the Gaussian charge distribution parameter α is set to 0.431 35 Å^{-1} in accordance with the general suggestion[30] ($5.37/L$), with L = 12.4255 Å being the length of the simulation box. We consider 64 water molecules equivalent to a density of 0.99 g/cm^3. The minimum image convention together with a spherical cutoff at half the box length is adopted for the short-

Table 1. Intramolecular Potential Parameters in SPCf Simulation

i	D_i/KJ mol^{-1}	α_i
1	549.0586	2.13498 Å^{-1}
2	414.5975	0.70337

ranged part of the potential. A time step of 1 fs is used for dynamics, and all velocity CFs are calculated up to 2.5 ps.

To derive an analytic expression for the smeared Hessian, we first decompose the total SPCf potential as

$$V_{H_2O} = V_{LJ}^{OO} + V_{Ewald} + V_{intra} \tag{27}$$

with

$$V_{LJ}^{OO} = 4\epsilon\left\{\left(\frac{\sigma}{r_{OO}}\right)^{12} - \left(\frac{\sigma}{r_{OO}}\right)^{6}\right\} \tag{28}$$

and

$$V_{Ewald} = V_{realspace} + V_{rec.space} - V_{self} - V_{molc.selfint.} \tag{29}$$

$$V_{intra} = V_{OH1} + V_{OH2} + V_{\Theta} = D_1\alpha_1^{\,2}(r_{OH1} - r_{eq})^2 + D_1\alpha_1^{\,2}(r_{OH2} - r_{eq})^2 + D_2\alpha_2^{\,2}(\Theta_{HOH} - \Theta_{eq})^2 \tag{30}$$

The Ewald real space part, reciprocal space part, and charge self-interaction and molecular self-interaction parts are given by[30]

$$V_{realspace} = \sum_i \sum_{j>i} q_i q_j \frac{erfc(\alpha r_{ij})}{r_{ij}} \tag{31}$$

and

$$V_{rec.space} = \frac{1}{2}\sum_{\mathbf{k}\neq 0}\sum_{i,j} 4\pi \frac{q_i q_j}{V||\vec{\mathbf{k}}||^2} \exp(-||\vec{\mathbf{k}}||^2/4\alpha^2)\exp[-i\vec{\mathbf{k}}(\vec{r}_i - \vec{r}_j)] \tag{32}$$

$$V_{self} = \frac{\alpha}{\sqrt{\pi}}\sum_i q_i^{\,2} \tag{33}$$

$$V_{molc.selfint.} = \sum_{pairs(i,j)} \frac{q_i q_j}{r_{ij}} erf(\alpha r_{ij}) \tag{34}$$

respectively. The parameter values for the intramolecular potential, D_1, D_2, α_1, and α_2, are listed in Table 1; these are obtained by requiring eq 30 to match the harmonic part of the local mode intramolecular potential of Reimers and Watts.[29] The values of r_{eq} and Θ_{eq} are however kept equal to their original SPC values:[28] an angle of 109.5° and a bond length of 1.0 Å. To proceed, we express the OH local mode intramolecular energy and oxygen LJ interactions in a "sum over Gaussian" form, that is

$$V_{OH_j} = \sum_{i=1,3} \beta_i \exp\left(-\frac{1}{2} r_{OH_j}^{\,2}/\zeta_i\right) + \zeta, \qquad j = 1, 2 \tag{35}$$

and

$$V_{LJ}^{OO} = \sum_{i=1,3} \gamma_i \exp\left(-\frac{1}{2} r_{OO}^{\,2}/\alpha_i\right) \tag{36}$$

Also, the Ewald real space part and Ewald molecular self-interaction term are put in a "sum over Gaussian" form by writing

$$\frac{erfc(\alpha r_{ij})}{r_{ij}} = \sum_{l=1,3} \delta_l \exp\left(-\frac{1}{2} r_{ij}^{\,2}/\eta_l\right) \tag{37}$$

and

$$\frac{erf(\alpha r_{ij})}{r_{ij}} = \sum_{l=1,2} \tau_l \exp\left(-\frac{1}{2} r_{ij}^{\,2}/\zeta_l\right) \tag{38}$$

respectively. The Gaussian parameters are collected in Table 2. The Gaussian representation of the classical electrostatic energy is tested by comparing its predicted energy to the energy of the original representation, eqs 31−34, for two randomly sampled configurations of the liquid. For this purpose, we use the MOSCITO 4 simulation package[30] with the same Ewald setup. An acceptable energy error of 0.1% was found for both geometries. Because Gaussian averages of multidimensional Gaussian and complex exponentials (the Ewald reciprocal space term) can be performed algebraically, see, for example, ref 24, it follows that $V_{H_2O,\underline{A}(\vec{z}_c)}$ and $\underline{\Omega}^2(\vec{z}_c)$ can be evaluated analytically, except for the intramolecular bending mode term, the latter being a function of all three water monomer atoms. To obtain the smeared Hessian and smeared potential of V_{Θ}, we adopt the following two approximations: First, the smeared Hessian of V_{Θ} is approximated by its classical Hessian, evaluated at the centroid. Second, we notice that the smeared potential, eq 16, may be expanded using the smearing width matrix as a smallness parameter:

$$V_{\Theta,\underline{A}(\vec{z}_c)} = V_{\Theta}(\vec{z}_c) + \frac{1}{2}\sum_{i,j} \underline{A}(\vec{z}_c)_{i,j} \frac{\partial^2}{\partial z_{c,i}\partial z_{c,j}} V_{\Theta}(\vec{z}_c) + \ldots \tag{39}$$

Obviously, if we truncate after the first nontrivial term, being linear in the smearing width matrix, we obtain an expression that requires only the analytic *classical* Hessian of the bending mode potential. Both approximations are exact for harmonic systems and for high temperatures. The Gaussian potentials in eqs 35−38 were also adopted in the classical propagation part of the LPI procedure.

We use two cycles, i−iii, of the FK iterative equations (section 2.3); for each cycle, the 576 × 576 effective frequency matrix is diagonalized. After self-consistency has been reached, the centroid potential and Wigner-transformed quasi-density operator are obtained, see eqs 15, 17−19 or ref 9 for more details. The temperature T is set to 296 K.

The integration over centroid positions, compare eq 4, is done by Metropolis MC,[31] utilizing the centroid density as a weight function. The trial moves involve simultaneous displacements of *all* atoms and are decomposed by the following sequential operations: (i) a uniform random translation of each atom, (ii) a uniform random rotation of

Table 2. Gaussian Fit Parameters Used in SPCf Simulation[a]

i	1	2	3
β_i/Hartree	7.1122	−8.73264	1.12917
γ_i/Hartree	1.77205	2.13115	89.459
δ_i/bohr^{-1}	0.19716251	0.3483857	0.088230
τ_i/bohr^{-1}	0.10209604	0.15546671	
ζ_i/bohr^2	2.14823	2.81753	3.1732
α_i/bohr^2	2.1315	13.4881	1.11393
η_i/bohr^2	3.36579	1.3012714	7.443253
ς_i/bohr^2	13.79489	101.44204	

[a] The value of ζ in eq 35 is $\zeta = 0.892\,724$ Hartree.

each molecule, (iii) a uniform random translation of each molecule, and finally (iv), again, a uniform random translation of each atom. Thus, the transition probability for trial configurational moves is symmetric in the configurational state, and we may utilize the usual Metropolis criterion for acceptance; see page 121 of ref 31. The step parameters are 0.0104 Å, 0.0334 rad, and 0.00175 Å for center-of-mass translation, rotation, and atomic translation, respectively.

To estimate the uncertainties in the calculated quantities, both classical and quantum calculations are repeated using 10 (7) different equilibrated initial water configurations for the classical (quantum) simulations. For the quantum simulations, 90 000 MC centroid steps are utilized to equilibrate the liquid, starting from a classical equilibrium geometry. For the production runs, for each geometry, the number of centroid MC steps is about 30 000−45 000 for the quantum calculations and 45 000−90 000 for the classical simulations. For each 20th configuration, the corresponding Wigner-transformed QDO is constructed and 10 sets of position and momenta are sampled for subsequent classical dynamics. For the quantum calculations, 45 000 MC samplings took approximately 6 days using a computer equipped with a single AMD 2.2 GHz Opteron processor.

3.2. He(4) Model. The calculation of the spectrum of density fluctuations for He(4) is done at 27 K and a density of 0.25 g/cm^3. The considered **Q** vector is 1.64 Å^{-1}. The liquid model/calculation is exactly as that in ref 6. That is, the He(4)−He(4) interactions are determined by the HFD-B2 potential of Aziz and co-workers,[32] which is rewritten as a sum over Gaussian functions to derive analytical expressions for eqs 11 and 16. The new calculation differs however from the original calculation in one significant way: instead of 64 He(4) atoms, we now consider 57 atoms, which makes the Laue equation exactly fulfilled. The new 57 atom box length is 11.494 Å, and hence, $\mathbf{Q} = 1.64$ Å^{-1}. The Laue condition was only approximately satisfied in the old work.[6]

We perform three different calculations, which use (i) the original analytical Gaussian-fit code,[6] (ii) the Hessian sampling strategy, and (iii) the gradient procedure, eqs 20−23. Both numerical methods, ii−iii, still utilize the Gaussian representation of the He(4) potential, so that any discrepancy between results of i and ii−iii may be ascribed to shortcomings of the new numerical implementations. In method ii, 160 and 1000 Box−Mueller samplings are adopted to evaluate eqs 11 and 16, respectively, while in method iii, 2500 and 1000 Box−Mueller samplings are adopted to evaluate eqs 22 and 16, respectively. We utilize $3 \times 300\,000$ centroid MC steps for methods i and ii, while 135 000 centroid MC steps were performed for the more time-consuming method iii.

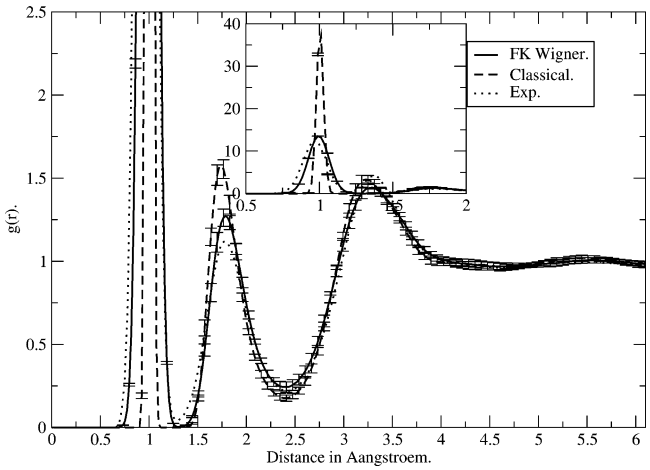

Figure 1. Radial distribution function gOH(r) for SPCf water model, evaluated via alternative methods, as indicated in the legend. Experimental data from ref 33.

These calculations are performed on a single computer equipped with a single 2 GHz Xeon processor. The analytic and the Hessian sampling codes use less than 1 week for 300 000 MC steps including classical dynamics, while the gradient sampling implementation requires about 30 days to perform 135 000 centroid MC steps (including dynamics).

4. Results

In this section, we present the structural and dynamic results of the water and He(4) simulations.

4.1. Equilibrium Properties of the Water Model. As in ref 7, one may consider the distribution of the FK effective frequencies and compare it with the density of classical instantaneous normal-mode frequencies. The result for the present model is, practically speaking, identical to the distribution given earlier for the 32-molecule study.[7] This means that the FK Wigner transform is well-defined for all centroid positions. As discussed in ref 7, for the vast majority of cases with one or more imaginary FK frequencies, the equations provide no ambiguity, and for the rare cases that do, a natural assignment (of zero momentum) is available for that mode.

The classical, FK Wigner-based, and experimental[33] radial distribution functions (RDFs) for O−H and O−O atom pairs, gOH(r) and gOO(r) are shown in Figures 1 and 2, respectively. While these results can be obtained essentially exactly via path integral Monte Carlo simulation (see, for example, ref 34), here, these calculations test the accuracy of the effective frequency local harmonic approximation. As is evident, the general trend is that which is expected: the quantum water RDFs are less structured and the peaks are shifted to longer distances as compared to those of the classical RDFs.[21] Beginning with gOH(r), we see that the Wigner-based gOH(r) agrees well with the experimental

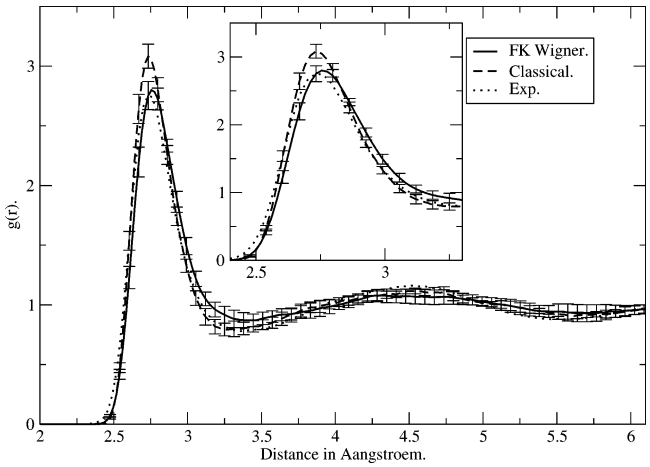

Figure 2. Radial distribution function *g*OO(*r*) for SPCf water model, evaluated via alternative methods, as indicated in the legend. Experimental data from ref 33.

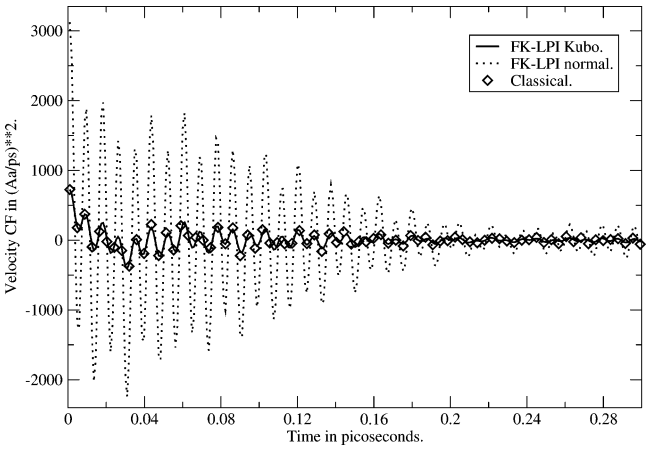

Figure 3. Classical, normal FK-LPI, and FK-LPI Kubo hydrogen velocity correlation functions for SPCf water model.

*g*OH(*r*). Not only are the experimental and Wigner intramolecular distributions (at about 1 Å) in good agreement with each other, so are the peak heights of the next two peaks, corresponding to the two hydrogen atoms belonging to a water molecule in the first solvation shell. More specifically, classically, the first intermolecular peak is higher than the second, whereas both the quantum and experimental RDFs predict the reverse order for amplitudes. This is because the closer, hydrogen-bonded, H at about 2 Å is broadened significantly by zero-point effects. From Figure 2, we observe that *g*OO(*r*) matches reasonably with the height of the experimental first peak, while the classical RDF exaggerates the structure of the liquid.

4.2. Dynamical Results for Water Model. *4.2.1. Diffusion.* We start by considering the diffusion coefficient *D* of liquid water, which can be extracted from the oxygen or hydrogen velocity CF (VCF) through the transport coefficient expression

$$D = \frac{1}{3}\int_0^\infty \mathrm{d}t\, \langle \vec{v}(t)\vec{v}(0)\rangle \tag{40}$$

In Figure 3, we display the hydrogen atom VCF obtained directly from the FK-LPI approximation and also by classical MD. We further show the so-called Kubo-transformed VCF as calculated by FK-LPI.[8] This special VCF resembles the classical VCF in many respects: it is real-valued, and it shares the same initial value as its classical counterpart. Still, the integrated Kubo-transformed VCF yields the correct quantum, not the classical diffusion coefficient, see refs 8 and 12. From Figure 3, we observe the larger initial amplitude of the FK-LPI normal VCF as compared to the formally equal values for the classical and Kubo FK-LPI VCF. The intramolecular motion is also much more visible in the FK-LPI normal VCF, a fact which may be ascribed to zero-point motion.

In Table 3, the values for *D* obtained from classical MD, FK-LPI, and the FK-LPI Kubo VCF are presented. All values are extracted using the oxygen VCF. We show also the value of *D* reported by Lobaugh and Voth,[35] using CMD with two flexible SPC potentials (SPC/F and SPC/F2), and by Miller and Manolopoulos,[4] employing RPMD with the rigid SPC/E potential. First, we observe the required consistent agreement between the two FK-LPI diffusion coefficients, which are also identical, within statistical accuracy, to the values obtained from integrating the hydrogen atom Kubo and normal VCFs. A straightforward comparison between the FK-LPI and CMD/RPMD values are difficult for several reasons. First, the *D*s depend—not surprisingly—on the chosen water potential. This is clearly illustrated by considering the results of the SPC/F and SPC/F2 potentials, which differ only by the form of their intramolecular force field. As seen from Table 3, there is a large difference between the classical *D*s obtained from these potentials. Second, as shown by Yeh and Hummer,[36] *D* increases linearly with the negative inverse of the box length, and using the viscosity of the liquid, one should first extrapolate to infinite system size in order to establish a correct model value for *D*. In this connection, it is interesting to note that Miller and Manolopoulos[4] found that the *ratio* of quantum to classical diffusion coefficients is almost constant as a function of the system size. Perhaps, this ratio is also the most interesting quantity when comparing quantum and classical models, because the models here do not produce an accurate agreement with the experiment. In any case, it appears that the quantum effect predicted by FK-LPI is somewhat larger than that for the other methods.

4.2.2. Spectrum of the Hydrogen Velocity CF and Dipole Moment Quantum Correction Factor. The water IR spectrum can be obtained once the water total system dipole moment CF, $\langle \vec{M}(t)\vec{M}(0)\rangle_{\mathrm{QM}}$, has been computed,[38,39] for example, via a FK-LPI calculation. However, even on a classical level, the calculation of $\langle \vec{M}(t)\vec{M}(0)\rangle_{\mathrm{CL}}$ converges rather slowly,[37] and it is therefore desirable to circumvent a direct FK-LPI attack on this CF. As shown by Marti and co-workers,[37] one may utilize the hydrogen atom VCF for mimicking the total system dipole moment derivative CF for water, $\langle \dot{M}(t)\dot{M}(0)\rangle_{\mathrm{QM}}$. In this approximation, the ratio—or QCF $Q(\omega)$—between the quantum and classical absorption spectra is identical to the ratio between the quantum FK-LPI and classical hydrogen VCF spectra:

Table 3. Water Diffusion Coefficients Obtained from Various Methods[a]

	RPMD(SPC/E)[b]	FK-LPI(SPCf), 64 molecules	CMD(SPC/F)[c]	CMD(SPC/F2)[c]
D/qm	0.43	0.50 ± 0.06/0.49 ± 0.06[d]	0.42	0.38
D/cl	0.29	0.23 ± 0.06	0.3 ± 0.02	0.22 ± 0.02
ratio	1.48	2.2/2.1	1.4	1.7

[a] Units Are Å²/ps [b] Data from ref 4 extrapolated to infinite system size. [c] Data from ref 35, using 125 molecules. [d] Two quantum values are the values obtained from FK-LPI Kubo and normal oxygen VCF, respectively.

$$Q(\omega) = \frac{\int \mathrm{d}t \exp(i\omega t)\langle \vec{M}(t)\vec{M}(0)\rangle_{\mathrm{QM}}}{\int \mathrm{d}t \exp(i\omega t)\langle \vec{M}(t)\vec{M}(0)\rangle_{\mathrm{CL}}} = \frac{\int \mathrm{d}t \exp(i\omega t)\langle \dot{M}(t)\dot{M}(0)\rangle_{\mathrm{QM}}}{\int \mathrm{d}t \exp(i\omega t)\langle \dot{M}(t)\dot{M}(0)\rangle_{\mathrm{CL}}}$$

$$\approx \frac{\int \mathrm{d}t \exp(i\omega t)\langle \vec{v}_{\mathrm{H}}(t)\vec{v}_{\mathrm{H}}(0)\rangle_{\mathrm{FK-LPI}}}{\int \mathrm{d}t \exp(i\omega t)\langle \vec{v}_{\mathrm{H}}(t)\vec{v}_{\mathrm{H}}(0)\rangle_{\mathrm{CL}}} \equiv Q_{\mathrm{FK-LPI}}(\omega) \tag{41}$$

$Q_{\mathrm{FK-LPI}}(\omega)$ is relatively inexpensive to obtain because it requires only a FK-LPI simulation of a single particle property. Knowing $Q_{\mathrm{FK-LPI}}(\omega)$, thus, enables us to extract the quantum IR spectrum by performing only a classical simulation of the water total system dipole moment CF.

Referring to Figure 3, one sees that the Kubo and classical hydrogen VCF are rather close to each other. A comparison of the Fourier transform (spectrum) of the quantum hydrogen VCF as predicted by the FK-LPI VCF and the same function as derived from the FK-LPI Kubo-transformed VCF is informative. A standard Fourier relation may be used to map the FK-LPI Kubo VCF spectrum onto the normal VCF spectrum, see ref 40. Hence, the normal VCF spectrum can be obtained in two ways: directly or indirectly. For an exact theory, these two spectra would be identical. Here, the consistency is an important internal test of the theory, as there is no formal requirement that the two power spectra agree in a given approximation. In Figure 4 is shown a comparison between the classical hydrogen VCF spectrum, the normal FK-LPI hydrogen VCF spectrum, and the normal hydrogen VCF spectrum obtained from the FK-LPI Kubo hydrogen VCF. Clearly, good agreement between the two FK-LPI spectra is observed, especially at higher frequencies. The two FK-LPI spectra agree completely in the bending and OH stretching regions (the latter is not shown) of the spectrum, an observation which is consistent with the fact that the underlying FK-LPI theory is exact for harmonic potentials.

As discussed above, the ratio between the classical and FK-LPI hydrogen VCF spectrum may be used to define a FK-LPI QCF, $Q_{\mathrm{FK-LPI}}(\omega)$. We apply $Q_{\mathrm{FK-LPI}}(\omega)$ as a multiplicative correction to the infrared spectrum obtained from classical molecular dynamics. We apply $Q_{\mathrm{FK-LPI}}(\omega)$, obtained using the Kubo VCF for H, to the infrared spectrum reported by Jeon et al.,[41] who utilized a particular flexible SPC variant, often referred to as SPC/F.[42] The computed and experimental[43] IR spectra are shown in Figure 5, where also the spectrum obtained by applying (i) no correction (classical) and (ii) a correction based on the so-called harmonic QCF has been displayed; the last of which has very recently been

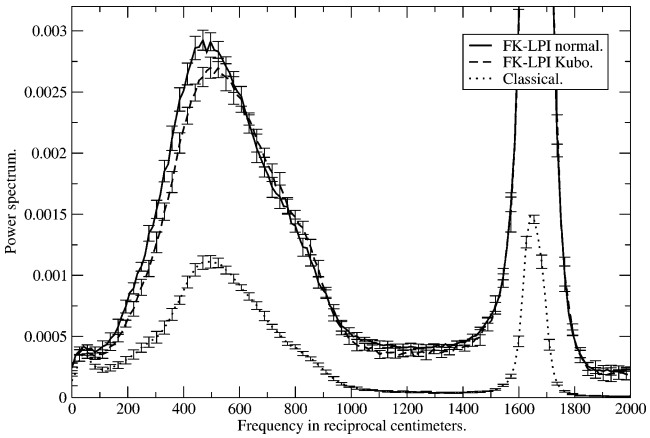

Figure 4. Spectra of hydrogen velocity correlation functions derived from classical, normal FK-LPI, and FK-LPI Kubo velocity correlation functions.

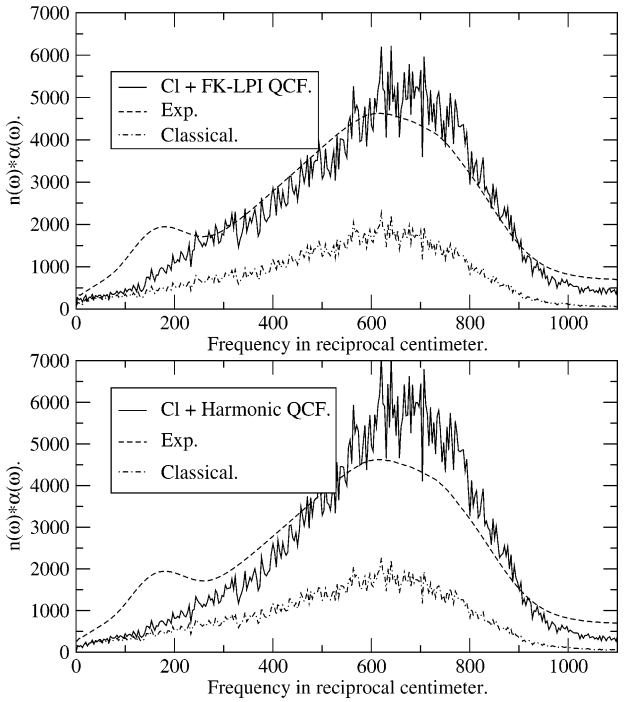

Figure 5. Comparison between water IR spectra derived by combining FK-LPI or "harmonic" quantum correction factors with the IR spectrum reported by Jeon et al.[41] obtained from classical molecular dynamics.

utilized to correct the IR spectrum of water.[38] The FK-LPI QCF is seen to perform better than the harmonic QCF, although the latter is clearly reasonable as a correction to the pure classical prediction. We emphasize that the FK-LPI QCF is computed ab initio and is determined only by the potential model chosen for water.

Table 4. Moments of the Van Hove Spectrum via Alternate Routes

	analytic[a]	Hessian numer.[a]	gradient[a]	Van Hove CF[b]	exptl.[c]	classical
$\langle\omega^1\rangle$/cm^{-1}	11.0	11.0	11.1	10.4	11.37	0
$\langle\omega^2\rangle$	1.9	1.9	1.9	1.7	1.8	1
$\langle\omega^3\rangle$/meV^2	134	134	131	107	123 ($Q = 1.63$ Å^{-1})	

[a] Alternative sampling methods are "analytic", analytical evaluation of averaged Hessian, eq 11; "Hessian, numer.", numerical average of analytical Hessian; "gradient", numerical average of position-weighted potential gradient, eq 22. [b] Data from ref 6. [c] Data from ref 27.

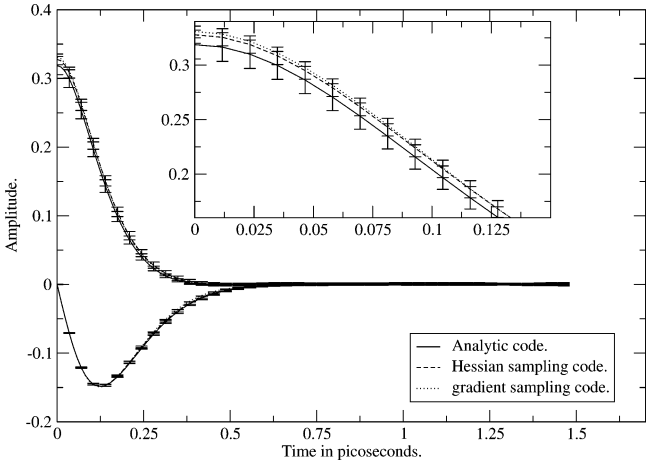

Figure 6. He(4) Van Hove correlation functions obtained from analytical Gaussian-fit, "Hessian sampling", and "gradient sampling" codes. The upper and lower set of lines represent the real and imaginary parts of the CFs, respectively. The insert expands part of the upper set of lines. In the lower set, the lines fall on top of each other.

4.3. Van Hove Spectrum of Liquid He(4). We now consider the alternative numerical approaches to FK-LPI. In Figure 6 is shown the calculated Van Hove CF for all three implementations defined in section 3.2. All CFs were calculated up to 1.5 ps. Very good agreement is seen. We note that all of the methods agree within their variances, estimated from three individual 300 000-step calculations. As in ref 6, one may calculate the linear, quadratic, and cubic moments of the Van Hove CF as a test of accuracy. The procedure fits the real part of the CF to a sum over Gaussians, and then, the moments are found from eqs 30 and 12 in ref 6. The moments are listed in Table 4, where we also report the moments obtained by applying the same fitting procedure to the original Van Hove CF data in ref 6. From the table, one sees very good agreement between the experiment[27] and FK-LPI calculations. The classical values for the first and second moments (last column) reflect the size of the quantum effect. Also, we see that the new FK-LPI moments are in slightly better agreement with the experiment than the previously published values;[6] a fact that most likely is caused by the exact fulfillment of the Laue equation in the present work.

5. Conclusion and Outlook

In this paper, we have applied the FK-LPI approximation to CFs for models of water and He(4) in their liquid states. The water structural results are in reasonable agreement with experimental data, indicating that the FK-LPI local harmonic approximation is a good one. The water quantum diffusion coefficients agree fairly well with CMD/RPMD simulations of similar water models, although the FK-LPI gives somewhat larger quantum effects. A consistency test is available for the FK-LPI case. It was found that the diffusion coefficients obtained from a direct calculation of the hydrogen or the oxygen atom velocity CFs agree very well with the values derived from a calculation of the Kubo-transformed CFs, which suggests that the values derived are accurate. The values must only be the same for an exact theory.

The He(4) Van Hove spectrum has been calculated using both a previously published implementation and two new and more general implementations of the FK-LPI theory. The results are, practically speaking, independent of the implementation and in very good agreement with the experiment. These explicitly demonstrate the computational feasibility of "black box" implementations of the underlying iterative Feynman−Kleinert equations, thereby enabling a general and simple coding of the theory.

The Hessian sampling approach has been demonstrated to be highly efficient, and for nonpolarizable potentials, where one has expressions for the classical Hessian, this implementation is efficient. The number of required samplings in eqs 11 and 16 would actually be *smaller* for water than for He(4), because the components of the smearing width matrix are smaller for water. The largest diagonal values for water are the hydrogen entries, $\sim$0.01 Å^2, while those for He(4) $\sim$ 0.03 Å^2. Hence, the sampling region in eqs 11 and 16 is simply smaller in the case of water.

The more general implementation is the gradient sampling technique, which only requires the classical potential and its gradient as input. Both are usual elements of any MD code. The results clearly show that the gradient implementation is slower than the Hessian sampling strategy, with eq 22 being the time-consuming part of the gradient calculation. However, it is immediately clear that this evaluation is highly suited for parallel computation. Hence, in terms of implementation, the gradient sampling approach also has this to recommend it.

Acknowledgment. J.A.P. and G.N. gratefully acknowledge support from the Swedish Research Council. P.J.R. gratefully acknowledges support from the National Science Foundation (CHE-0134775) and the Robert A. Welch Foundation. J.A.P. thanks Jonggu Jeon for sharing the SPC/F infrared spectrum with the authors.

References

(1) Jang, S.; Voth, G. A. *J. Chem. Phys.* **1999**, *111*, 2357−2370.

(2) Hone, T. D.; Voth, G. A. *J. Chem. Phys.* **2004**, *64*, 6412−6422.

(3) Craig, I. R.; Manolopoulos, D. E. *J. Chem. Phys.* **2005**, *121*, 3368−3373.

(4) Miller, T. F., III; Manolopoulos, D. E. *J. Chem. Phys.* **2005**, *123*, 154504.

(5) Nakayama, A.; Makri, N. *Proc. Natl. Acad. Sci. U.S.A.* **2005**, *102*, 4230−4234.

(6) Poulsen, J. A.; Nyman, G.; Rossky, P. J. *J. Phys. Chem. A* **2004**, *108*, 8743−8751.

(7) Poulsen, J. A.; Nyman, G.; Rossky, P. J. *Proc. Natl. Acad. Sci. U.S.A.* **2005**, *102*, 6709−6714.

(8) Poulsen, J. A.; Nyman, G.; Rossky, P. J. *J. Phys. Chem. B* **2004**, *108*, 19799−19808.

(9) Poulsen, J. A.; Nyman, G.; Rossky, P. J. *J. Chem. Phys.* **2003**, *119*, 12179−12193.

(10) Shi, Q.; Geva, E. *J. Phys. Chem. A* **2003**, *107*, 9070−9078.

(11) Rabani, E.; Reichman, D. R. *J. Chem. Phys.* **2004**, *120*, 1458−1465.

(12) Rabani, E.; Reichman, D. R.; Krilov, G.; Berne, B. J. *Proc. Natl. Acad. Sci. U.S.A.* **2002**, *99*, 1129−1133.

(13) Shi, Q.; Geva, E. *J. Chem. Phys.* **2003**, *118*, 8173−8184.

(14) Hernandez, R.; Voth, G. A. *Chem. Phys.* **1998**, *223*, 243−255.

(15) Wang, H.; Sun, X.; Miller, W. H. *J. Chem. Phys.* **1998**, *108*, 9726−9736.

(16) Causo, M. S.; Ciccotti, G.; Montemayor, D.; Bonella, S.; Coker, D. F. *J. Phys. Chem. B* **2005**, *109*, 6855−6865.

(17) Giachetti, R.; Tognetti, V. *Phys. Rev. Lett.* **1985**, *55*, 912−915.

(18) Feynman, R. P.; Kleinert, H. *Phys. Rev. A* **1986**, *34*, 5080−5084.

(19) Sun, X.; Miller, W. H. *J. Chem. Phys.* **1997**, *106*, 916−927.

(20) We note that a Boltzmann Wigner transform based on effective frequency theory has previously been considered by Cuccoli, Tognetti, Verrucchi, and Vaia in *Phys. Rev. A* **1992**, *45*, 8418−8429. We thank Ruggero Vaia for bringing this to our attention. However, their paper does not use the quasi-density operator formalism.

(21) Available quantum studies of water models predict an overall decrease in structure when quantum effects are included.[22,34] In an ab initio quantum MD study, Chen and co-workers[23] have observed generally comparable behavior to empirical models. However, they observed a more structured quantum OH radial distribution function, relative to classical, and rationalized this by an increase in polarity of the molecules, brought about by an increase in the anharmonic OH bond length when including quantum effects. We note that examination of such a quantum effect is not accessible in the present study, because the SPCf potential is harmonic in the OH stretch, and quantization of the nuclei will not change the bond lengths (in contrast to a Morse potential).

(22) Stern, H. A.; Berne, B. J. *J. Chem. Phys.* **2001**, *115*, 7622−7628.

(23) Chen, B.; Ivanov, I.; Klein, M. L.; Parrinello, M. *Phys. Rev. Lett.* **2003**, *91*, 215503.

(24) Cao, J.; Voth, G. A. *J. Chem. Phys.* **1994**, *101*, 6168−6183.

(25) Press, W. H.; Teukolsky, S. A.; Vetterling, W. T.; Flannery, B. P. In *Numerical Recipes*, 2nd ed.; Cambridge University Press: Cambridge, U. K., 1992.

(26) Lovesey, S. W. In *Theory of Neutron Scattering From Condensed Matter*; Oxford University Press: Oxford, U. K., 1986.

(27) Verbeni, R.; Cunsolo, A.; Pratesi, G.; Monaco, G.; Rosica, F.; Masciovecchio, C.; Nardone, M.; Ruocco, G.; Sette, F.; Albergamo, F. *Phys. Rev. E* **2001**, *64*, 021203.

(28) Berendsen, H. J. C.; Postma, J. P. M.; van Gunsteren, W. F.; Hermans, J. In *Intermolecular Forces*; Reidel: Dordrecht, The Netherlands, 1981.

(29) Reimers, J. R.; Watts, R. O. *Mol. Phys.* **1984**, *52*, 357−381.

(30) Paschek, D.; Geiger, A. *User's Guide and Manual MOSCITO 4*. http://ganter.chemie.uni-dortmund.de/MOSCITO (accessed Aug 10, 2006).

(31) Allen, M. P.; Tildesley, D. J. In *Computer Simulations of Liquids*; Oxford University Press: Oxford, U. K., 1987.

(32) Aziz, R. A.; Slaman, M. J.; Koide, A.; Allnatt, A. R.; Meath, W. J. *Mol. Phys.* **1992**, *77*, 321−337.

(33) Soper, A. K. *Chem. Phys.* **2000**, *258*, 121−137.

(34) Buono, G. S. D.; Rossky P. J.; Schnitker, J. *J. Chem. Phys.* **1991**, *95*, 3728−3737.

(35) Lobaugh, J.; Voth, G. A. *J. Chem. Phys.* **1997**, *106*, 2400−2410.

(36) Yeh, I.; Hummer, G. *J. Phys. Chem. B* **2004**, *108*, 15873−15879.

(37) Marti, J.; Guardia, E.; Padro, J. A. *J. Chem. Phys.* **1994**, *101*, 10883−10891.

(38) Iftimie, R.; Tuckerman, M. E. *J. Chem. Phys.* **2005**, *122*, 214508.

(39) McQuarrie, D. A. In *Statistical Mechanics*; Harper and Row: New York, 1976.

(40) Zwanzig, R. In *Nonequilibrium Statistical Mechanics*; Oxford University Press: New York, 2001.

(41) Jeon, J.; Lefohn, A. E.; Voth, G. A. *J. Chem. Phys.* **2003**, *118*, 7504−7518.

(42) Toukan, K.; Rahman, A. *Phys. Rev. B* **1985**, *31*, 2643−2648.

(43) Bertie, J. E.; Lan, Z. *Appl. Spectrosc.* **1996**, *50*, 1047−1057.

CT600167S